Supporting Information

Ruoyu Wang[1,2], Zhe Guo[1,2], Qiang Zhang[1,2], Jianfeng Cai[1,2], Guoqiang Liu [1,2,*], Xiaojian Tan[1,2,*], Jun Jiang[1,2,*]

[1]Ningbo Institute of Materials Technology and Engineering, Chinese Academy of Sciences, Ningbo 315201, China

[2] University of Chinese Academy of Sciences, Beijing 100049, China

E-mail: liugq@nimte.ac.cn; tanxiaojian@nimte.ac.cn; jjun@nimte.ac.cn

Figures

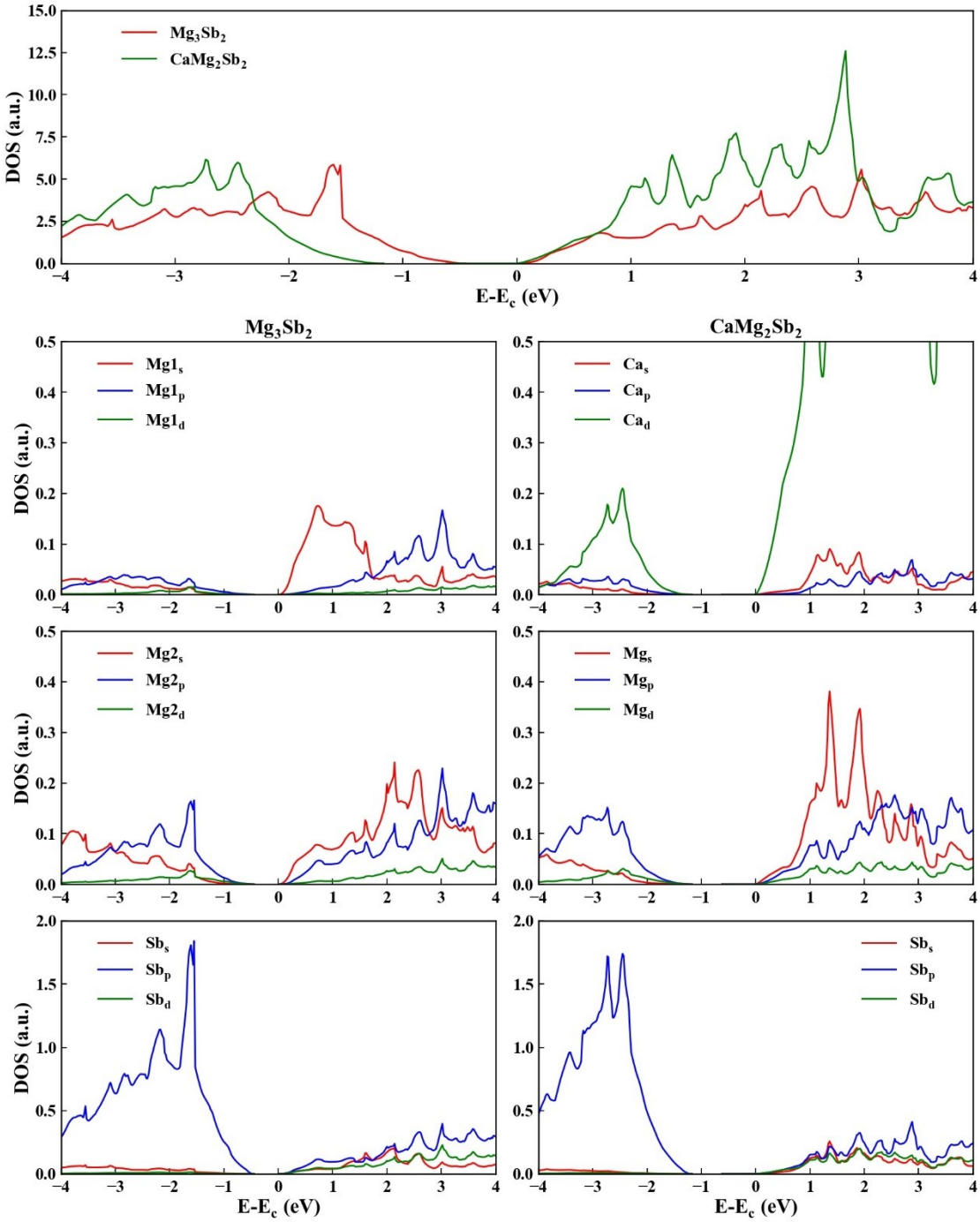

Figure S1. The total electronic density of states of $CaMg_2Sb_2$ and Mg_3Sb_2 (Upper). The atomic partial density of states of Mg_3Sb_2 (left column). atomic partial density of states of $CaMg_2Sb_2$ (right column).

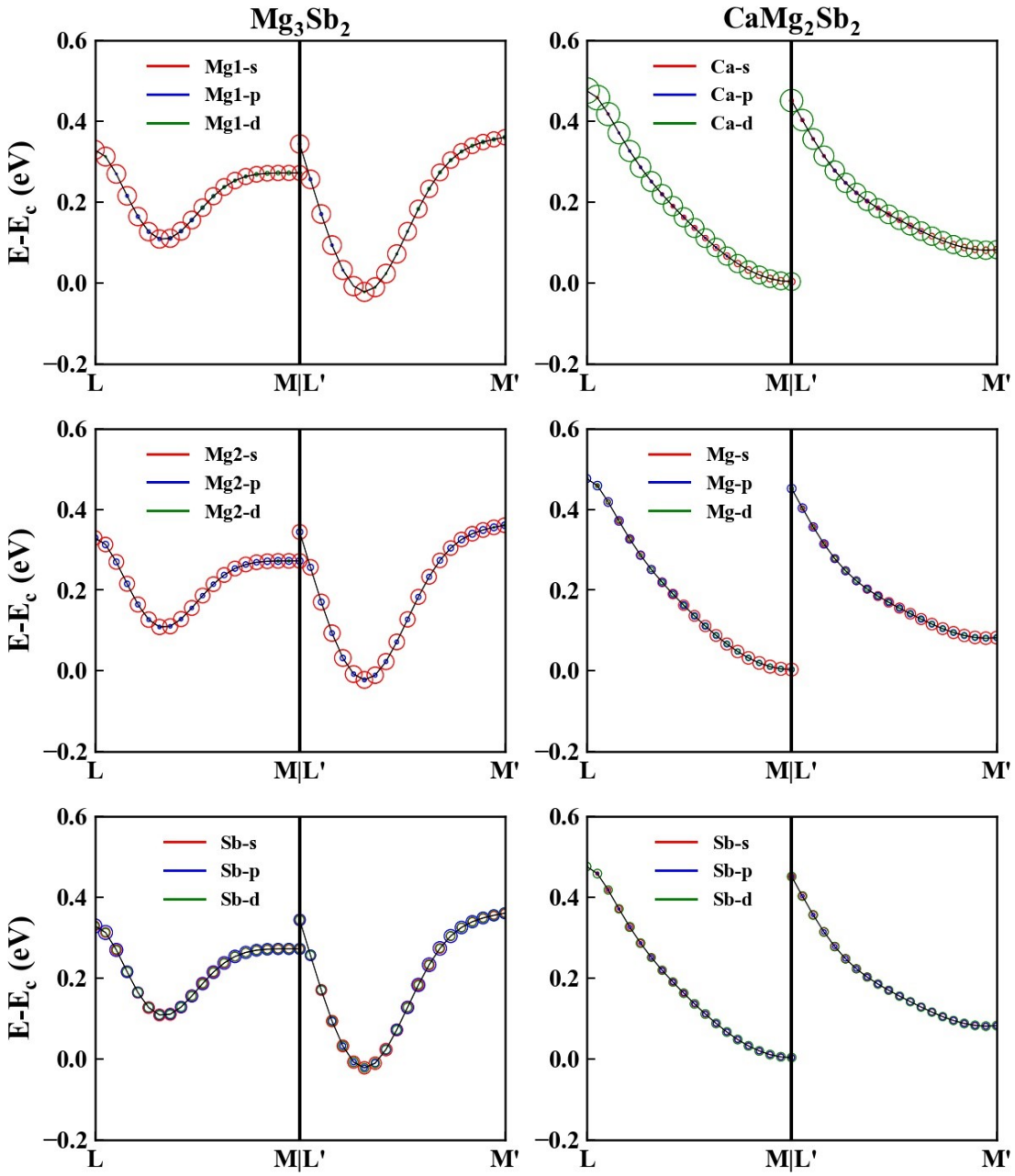

Figure S2. The projected electronic band structure for the conduction band edge of Mg_3Sb_2 and $CaMg_2Sb_2$.

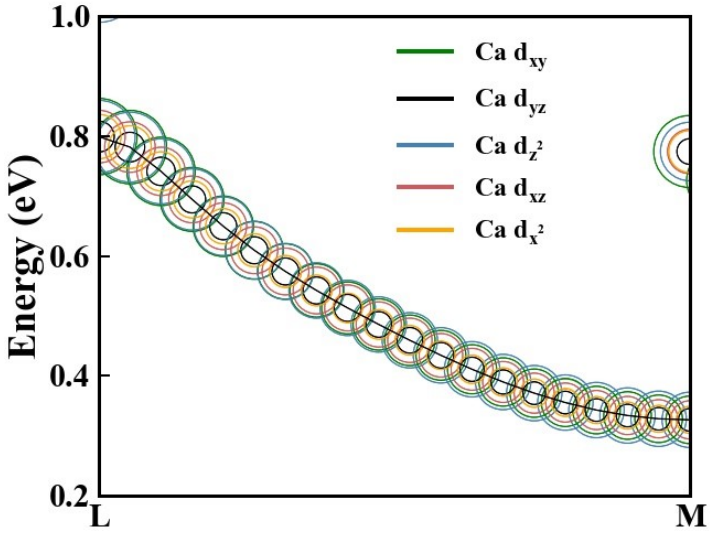

Figure S3. The projected band structure for the five Ca-*d* orbitals at the conduction band minimum of $CaMg_2Sb_2$ at the 'M' point. The three most significant components at M point are Ca-d_{z^2}, Ca-d_{xy} and Ca-d_{xz}, respectively.

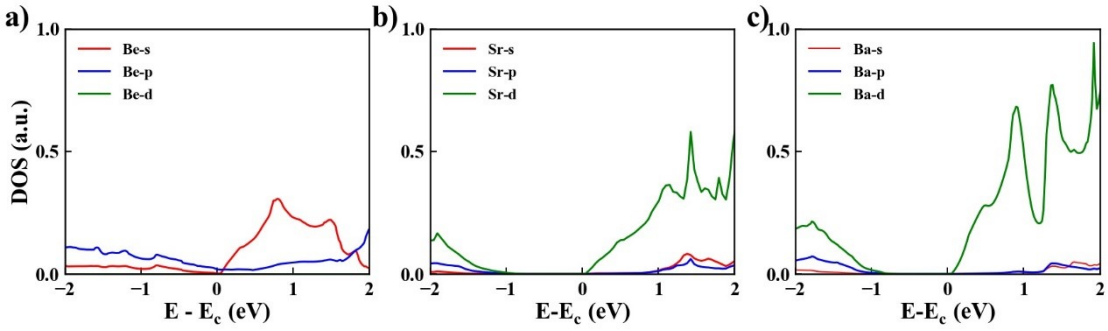

Figure S4. The partial density of states for the 'A'-site atom in $BeMg_2Sb_2$, $SrMg_2Sb_2$ and $BaMg_2Sb_2$, respectively.

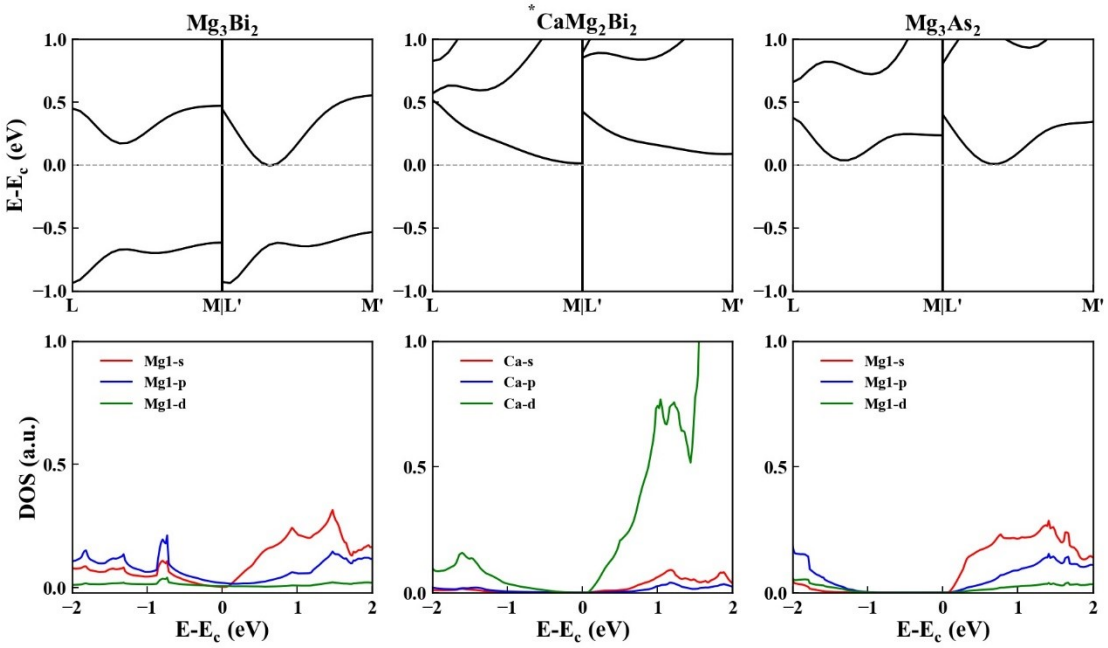

Figure S5. Band dispersion and partial density of states at the conduction band edge of Mg_3Bi_2, $CaMg_2Bi_2$ and Mg_3As_2. (Note: the CBM of $CaMg_2Bi_2$ is in fact located at the Gamma point. Here the CBM is set to the M point for consistency)

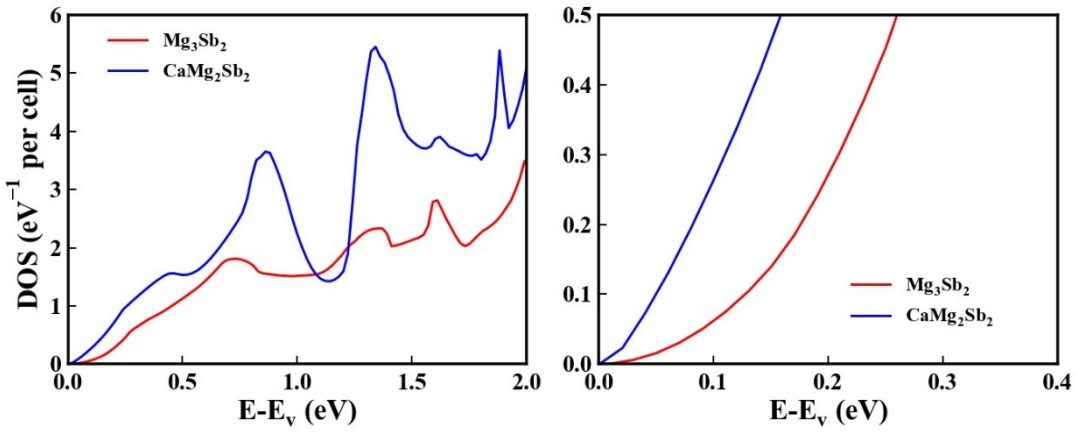

Figure S6. Comparison of total density of states of Mg_3Sb_2 and $CaMg_2Sb_2$ at conduction band edge.

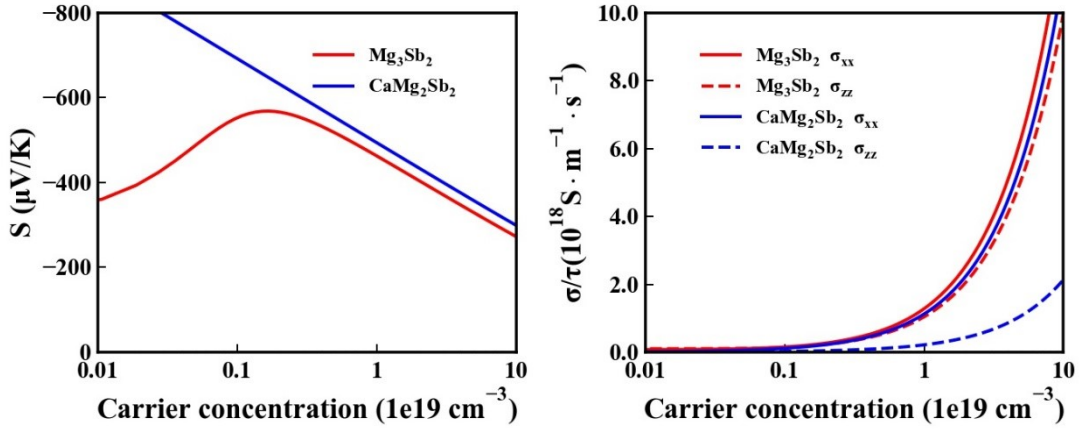

Figure S7. Seebeck coefficient and the electrical conductivity/relaxation time ratio of Mg_3Sb_2 and $CaMg_2Sb_2$ at 800 K.

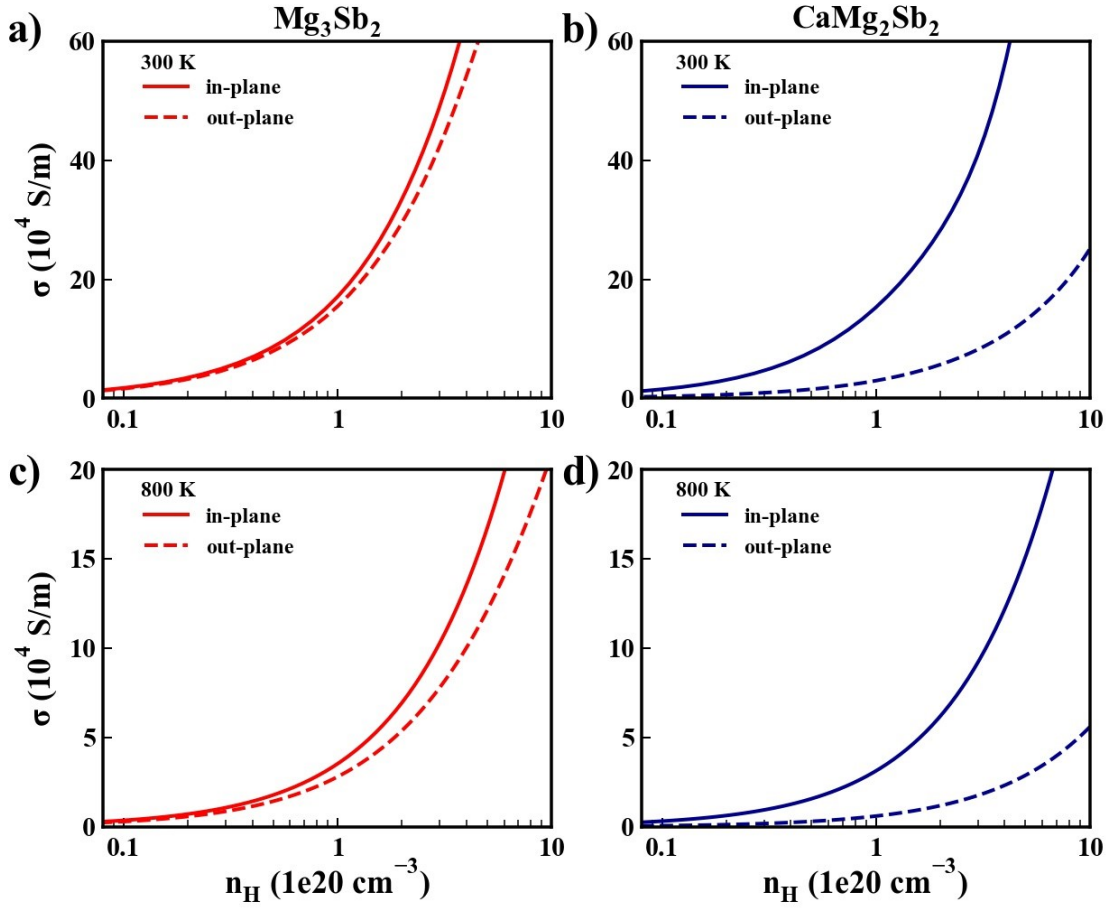

Figure S8. Estimated electrical conductivity of Mg_3Sb_2 and $CaMg_2Sb_2$. The in-plane and out-plane σ of Mg_3Sb_2 at (a) 300 K and (c) 800 K. The in-plane and out-plane σ of $CaMg_2Sb_2$ at (b) 300 K and (d) 800 K.

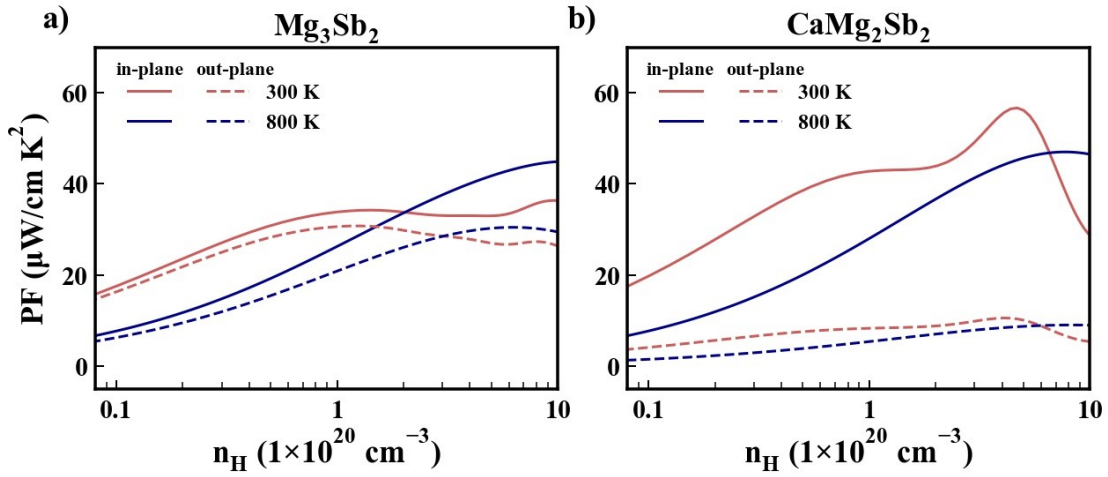

Figure S9. The estimated PF of (a) Mg_3Sb_2 and (b) $CaMg_2Sb_2$ at 300 and 800 K.

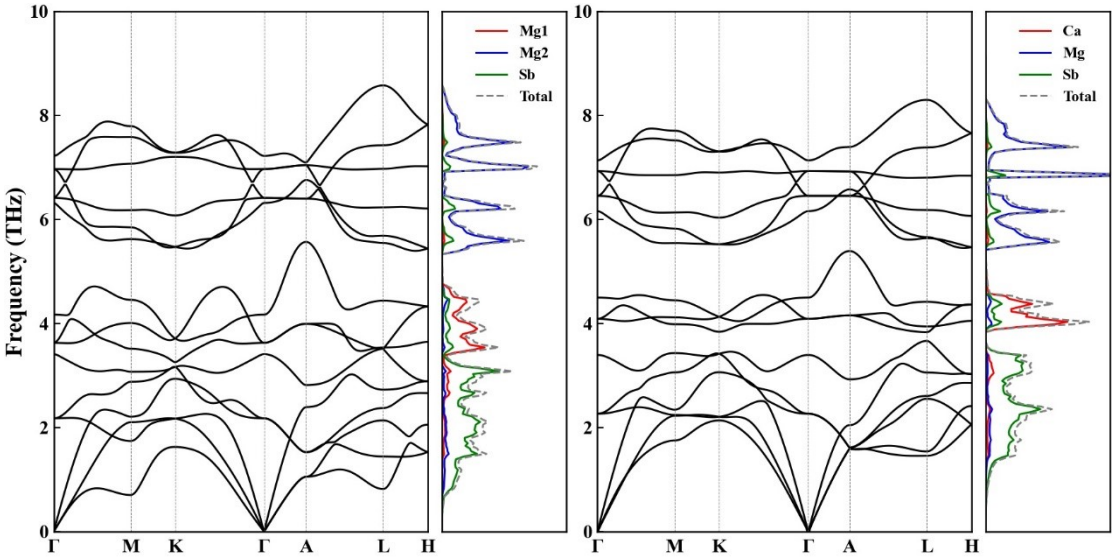

Figure S10. The phonon dispersion and projected density of states of Mg_3Sb_2 and $CaMg_2Sb_2$, respectively.

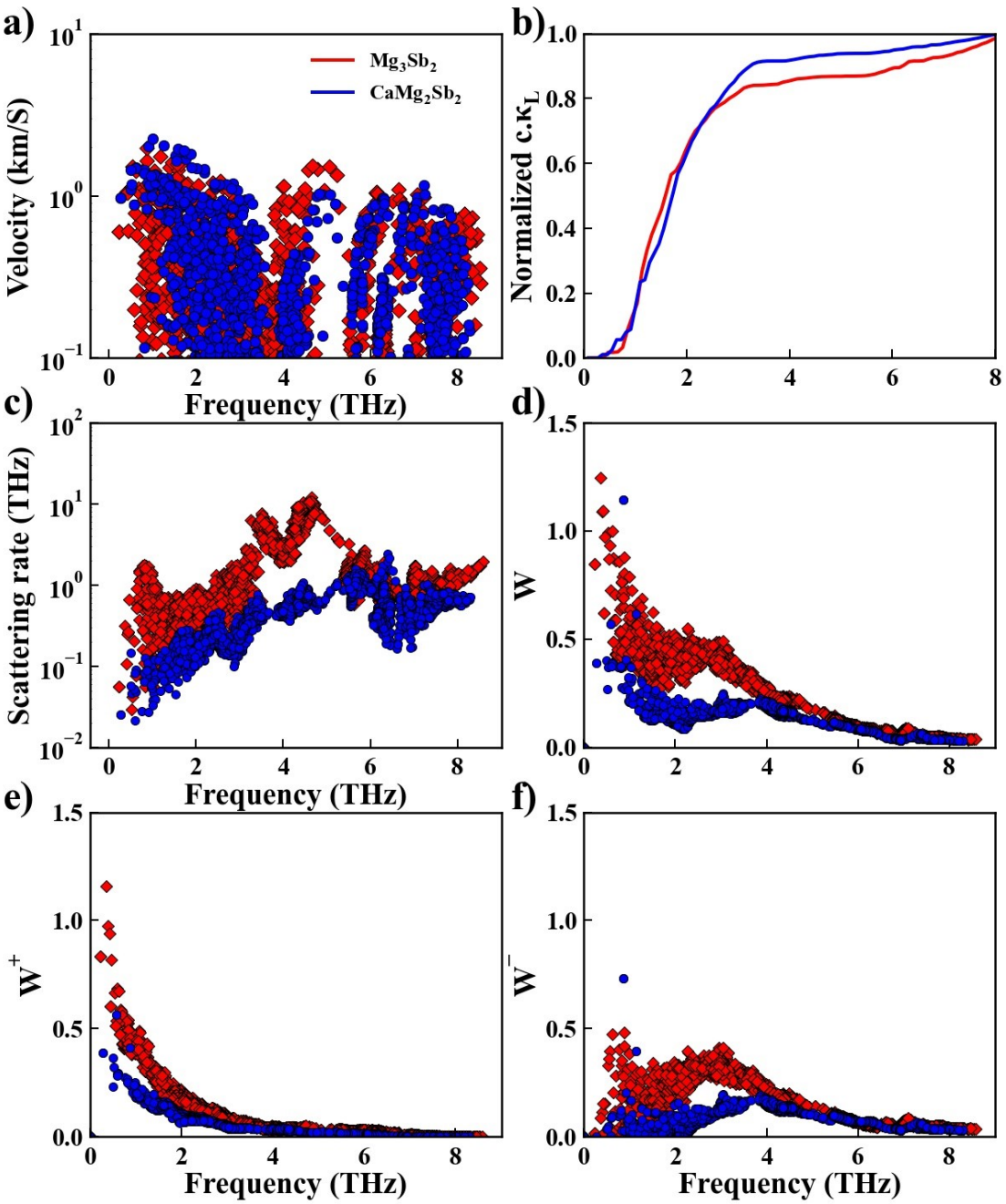

Figure S11. a) The sound velocity of Mg_3Sb_2 and $CaMg_2Sb_2$. b) The cumulative κ_l of Mg_3Sb_2 and $CaMg_2Sb_2$ normalized to their respective κ_l. c) Anharmonic scattering rate of Mg_3Sb_2 and $CaMg_2Sb_2$. d) The weighted scattering phase space of three-phonon processes. e) The weighted scattering phase space of three-phonon annihilation process. And f) the weighted scattering phase space of three-phonon absorption process.

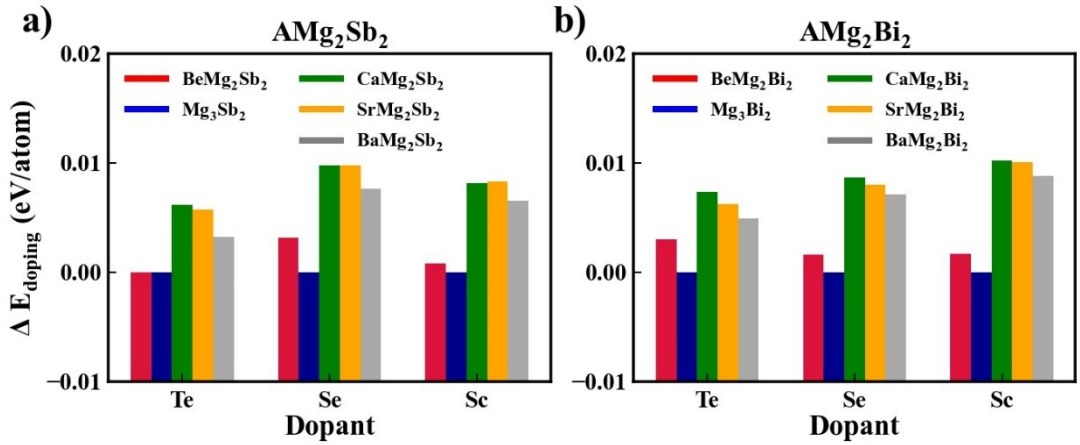

Figure. S12 Doping energy ΔE_{doping} of $BeMg_2X_2$ (X=Sb, Bi) compared with their AMg_2X_2 (A=Mg, Ca, Sr and Ba) counterparts. The ΔE_{doping} of $BeMg_2X_2$ significantly lower than $CaMg_2X_2$, $SrMg_2X_2$ and $BaMg_2X_2$, due to the absent *p-d* bonding.

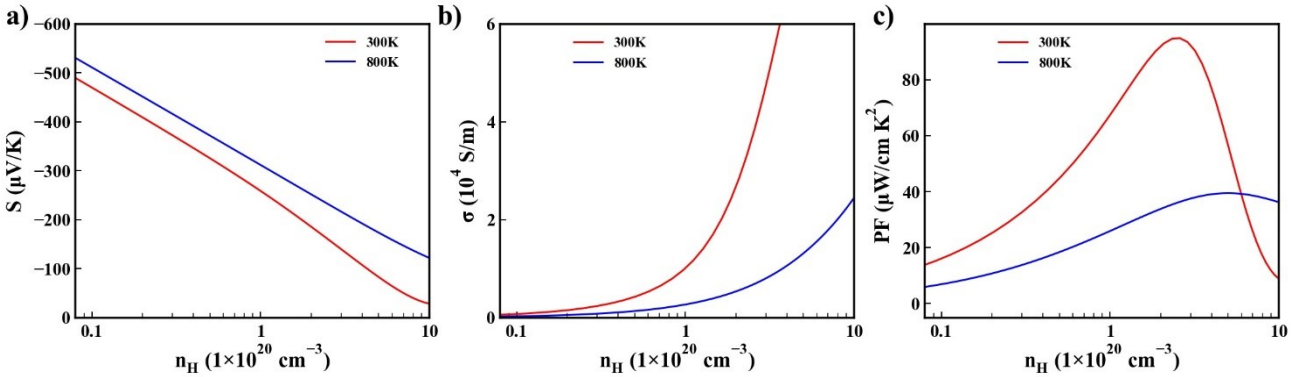

Figure S13. The estimated *in-plane* thermoelectric transport of $BaMg_2Sb_2$. a) Seebeck coefficient b) electrical conductivity and c) power factor.

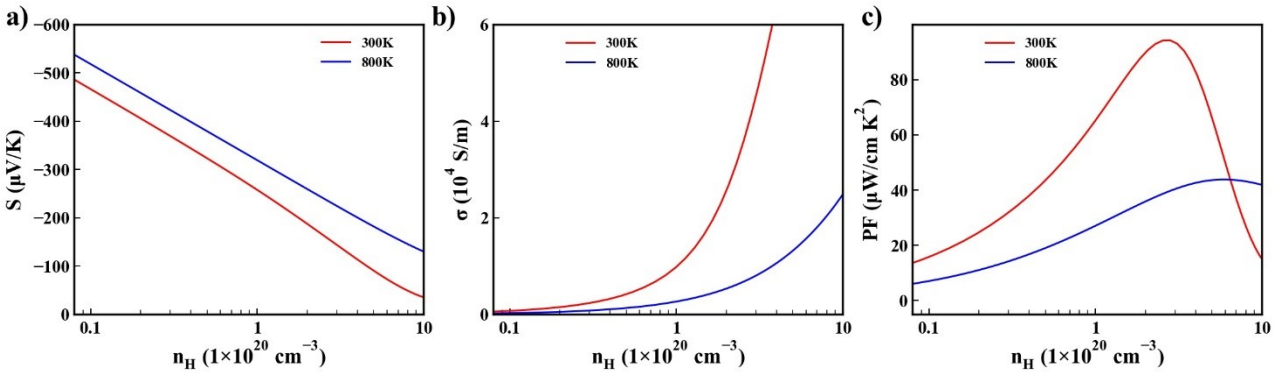

Figure S14. The estimated *in-plane* thermoelectric transport of $BaMg_2SbBi$ alloy. a) Seebeck coefficient b) electrical conductivity and c) power factor.

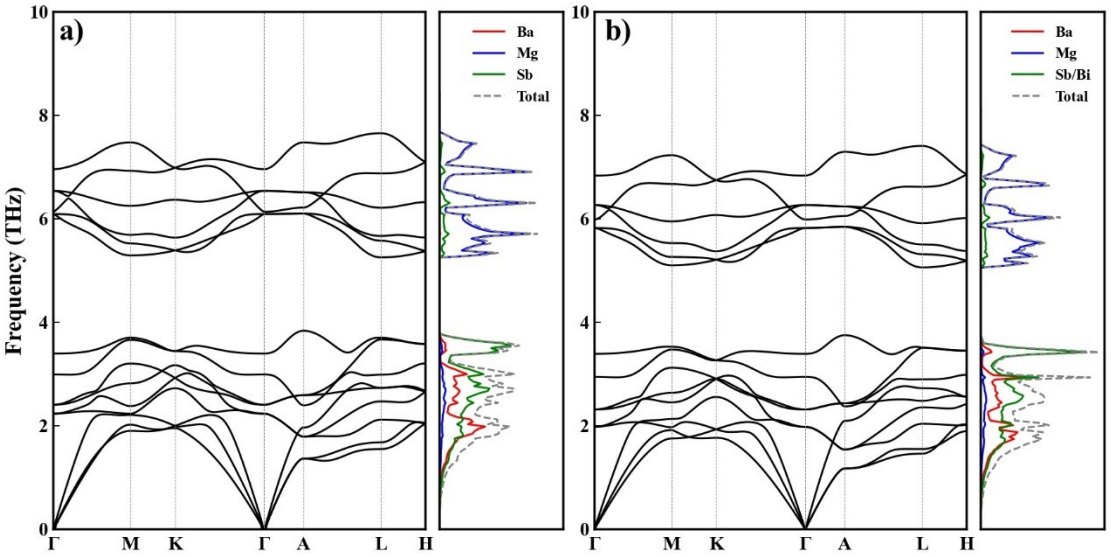

Figure S15. The phonon dispersion and projected density of states of $BaMg_2Sb_2$ and $BaMg_2SbBi$, respectively. The phonon dispersion of $BaMg_2SbBi$ is calculated using the "virtual crystal" technique.

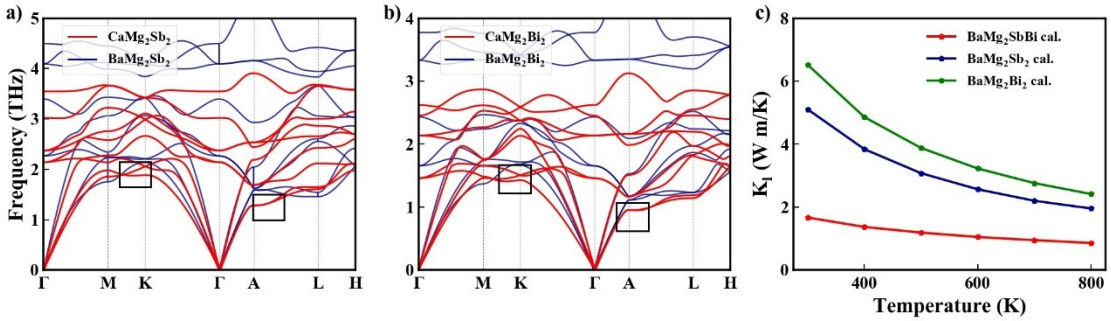

Figure S16. The phonon dispersion and calculated κ_L of $BaMg_2X_2$ (X=Sb, Bi). (a) The phonon dispersion spectrum of $CaMg_2Sb_2$ and $BaMg_2Sb_2$. Note that moderate band softening can be observed for $BaMg_2X_2$. (b) The phonon dispersion spectrum of $CaMg_2Bi_2$ and $BaMg_2Bi_2$. (c) The calculated of $BaMg_2Sb_2$, $BaMg_2Bi_2$ and $BaMg_2SbBi$ solid solution.

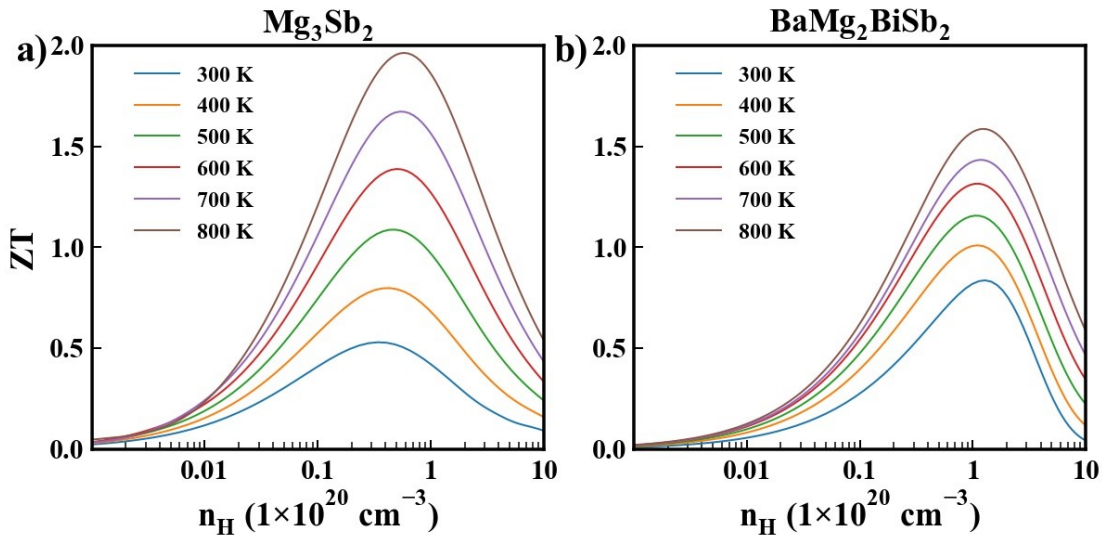

Figure S17. The estimated *in-plane* ZT values of Mg_3Sb_2 and $BaMg_2SbBi$.

Tables:

Table S1. The 2nd order IFC between Sb and up to the 3rd nearest neighbor in various AMg_2Sb_2 compounds. The unit of 2nd order IFC is $eVÅ^{-2}$

	P1(Sb-Mg)	P2 (Sb-Mg)	P3 (Sb-A)
MgMg2Sb2	2.32	2.18	0.59
CaMg2Sb2	2.60	2.16	1.13
BaMg2Sb2	2.45	2.21	1.11

Table S2. The electronic relaxation time extracted from the experimental electrical transport properties of Mg_3Sb_2 single crystal.[1]

Temperature (K)	300	400	500	600	700	800
τ (10^{-14} s)	1.23	0.80	0.57	0.44	0.34	0.28

Analysis of the *p-d* bonding in $CaMg_2Sb_2$

Figure S18 presents the PDOS of Ca-d and Sb-p orbitals in $CaMg_2Sb_2$. Clearly, the major peak of Ca-*d* orbital in the valence band is around -2.5 eV, where Sb-p orbital exhibits a higher peak with similar shape. The similar DOS peaks of Sb-p and Ca-d orbitals could also be observed in the conduction bands from 0 to 5 eV. The strong hybridization of the PDOS indicates a covalent-like bonding between Sb-p and Ca-d orbitals. Therefore, the DOS peak around -2.5 eV can be identified as a bonding state, and conduction band edge can be identified as an anti- bonding state.

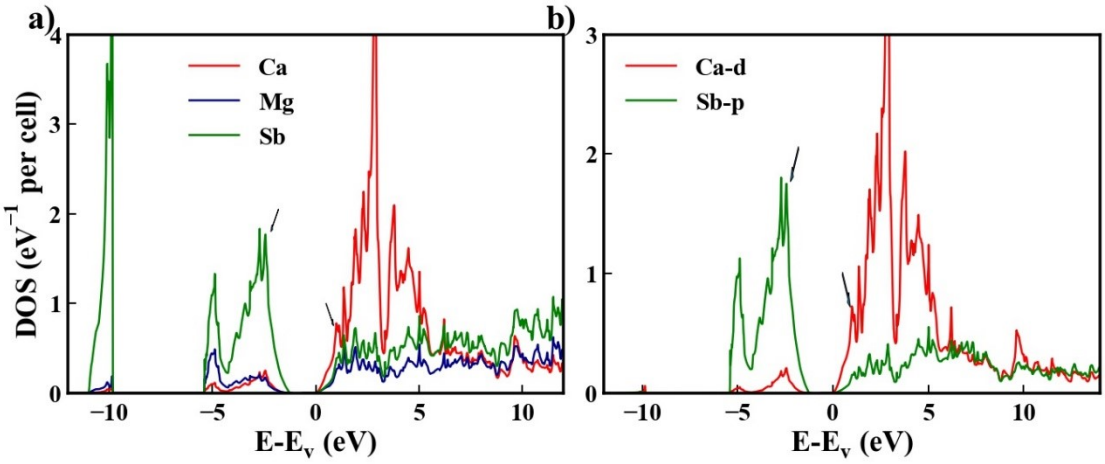

Fig. S18 Partial density of states of $CaMg_2Sb_2$. (a) Atomic PDOS of Ca, Mg and Sb atoms. (b) PDOS of Ca-*d* and Sb-*p* orbitals

Calculation details for the energy change upon doping.

The formation energy ($E_{formation}$) of a given compound can be written as:

$$E_{formation}=E_{compound}-\Sigma n_i E_{atom,i} \quad (1)$$

where $E_{compound}$ is the total energy of compound, and n_i and $E_{atom,i}$ are the number and energy of ith component atom in free space, respectively. The difference in $E_{formation}$ between two compounds can be calculated as the follows:

$$\Delta E_{formation}=\Delta E_{compound}-\Sigma \Delta n_i E_{atom,i} \quad (2)$$

When an atom in some pure substance is substituted for a dopant atom, the doping energy E_{doping} can be defined as following

$$E_{doping}=(E_{doped}-E_{pure})-(E_{atom,dopant}-E_{atom,a}) \quad (3)$$

The E_{doping} may indicate the level of difficulty in doping. A larger E_{doping} suggest the

doping be more difficult and *vice versa*. Though E_{atom} is not directly accessible within the framework of VASP package which has an arbitrary zero-point energy, we can still compare the doping of two different compound, provided that both the dopant element and the doping site are the same in the two compounds. Therefore, the relative doping energy of two compound, e.g., the Te doping at the Sb site for Mg_3Sb_2 and $CaMg_2Sb_2$, ΔE_{doping}, can be written as

$$\Delta E_{doping} = (E_{Te,Sb,CaMg2Sb2} - E_{pure,CaMg2Sb2}) - (E_{Te,Sb,Mg3Sb2} - E_{pure,Mg3Sb2}) \quad (4)$$

All terms in (4) are calculable with the VASP package.

For the specific calculation of ΔE_{doping} carried out in this work, the Te or Se dopant replace X site atom (Sb or Bi), whereas the Sc dopant substitutes the tetrahedrally coordinated Mg in AMg_2X_2.

Calculation details for the electrical conductivity σ and electrical thermal conductivity κ_e

The electronic transport properties of all phases are calculated using the Boltzmann transport theory with the rigid band approximation. The electrical conductivity is calculated by the equation $\sigma = (\sigma/\tau)\tau$, where τ denotes the relaxation time. The σ/τ can be calculated by solving Boltzmann transport equation (BTE), whereas τ is extracted from experimental measurement. Since there is no available experimental data for the n-type materials except $Mg_3(Sb, Bi)_2$, the relaxation time (τ) is extrapolated from the experimental value of the n-type Mg_3Sb_2 single crystal (Table S2) and applied to all other phases.[1] For the calculation of electronic thermal conductivity (κ_l), the Widemann-Franz relation ($\kappa_l = L\sigma T$) is used as an approximation, with the L chosen as the Sommerfeld value. Due to the *p-d* bonding, the n-type $CaMg_2Sb_2$ and $BaMg_2Sb_2$ exhibits anisotropic n-type electrical conductivity, and hence the anisotropic power factors, with the *in-plane* direction being more favored.

References

(1) Imasato, K.; Fu, C.; Pan, Y.; Wood, M.; Kuo, J. J.; Felser, C.; Snyder, G. J.

Metallic N-Type Mg_3Sb_2 Single Crystals Demonstrate the Absence of Ionized Impurity Scattering and Enhanced Thermoelectric Performance. *Adv. Mater.* **2020**, *32* (16), 1908218. https://doi.org/10.1002/adma.201908218.

(2) Tamura, S. Isotope Scattering of Dispersive Phonons in Ge. *Phys. Rev. B* **1983**, *27* (2), 858–866. https://doi.org/10.1103/PhysRevB.27.858.

(3) Pei, Y.; Gibbs, Z. M.; Gloskovskii, A.; Balke, B.; Zeier, W. G.; Snyder, G. J. Optimum Carrier Concentration in N-Type PbTe Thermoelectrics. *Adv. Energy Mater.* **2014**, *4* (13), 1400486. https://doi.org/10.1002/aenm.201400486.